

# Spatial dynamics, thermalization, and gain clamping in a photon condensate

Jonathan Keeling and Peter Kirton

*SUPA, School of Physics and Astronomy, University of St Andrews, St Andrews, KY16 9SS, United Kingdom*

(Dated: November 25, 2018)

We study theoretically the effects of pump-spot size and location on photon condensates. By exploring the inhomogeneous molecular excitation fraction, we make clear the relation between spatial equilibration, gain clamping and thermalization in a photon condensate. This provides a simple understanding of several recent experimental results. We find that as thermalization breaks down, gain clamping is imperfect, leading to spatial hole burning and multimode condensation. This opens the possibility of engineering the gain profile to control the condensate structure.

The laser has long served as a prototype for phase transitions in driven dissipative systems [1, 2]. While for a single-mode cavity the transition is mean-field-like, in a multimode cavity [3] spatial fluctuations are possible, enabling non-trivial critical behavior. Driven-dissipative phase transitions have been extensively studied in the last decade, motivated by experiments on polariton condensation [4–6]. These studies showed that features beyond the equilibrium classification [7] can arise, such as new critical exponents in three dimensions [8], and the destruction of algebraic order in two-dimensional systems [9].

Closely related to both polariton condensates and photon lasers are experiments on Bose-Einstein condensation (BEC) of photons [10] in organic-dye-filled microcavities. Unlike polaritons, these systems have no strong matter-light coupling and so the normal modes are non-interacting photons. However thermalization is possible [11] via the dye molecules. If a photon can be absorbed and emitted many times before it leaves the cavity, the photon gas achieves thermal equilibrium with the dye. Thus, by adjusting the rates of absorption and emission, or cavity decay, one may interpolate between an equilibrium BEC, and a strongly dissipative dye laser [12]. We will refer to condensation throughout this letter, but we present phenomena that can be interpreted either as lasing or BEC. Following these experiments many theoretical works [13–25] explored topics including equilibration, phase coherence, and photon statistics of the photon BEC, and later experiments studied photon statistics [26]. Recently, two experiments [27, 28] studied the spatial profile and dynamics of the photon BEC and their dependence on pump-spot size and location, observing behavior beyond the scope of existing models. Spatial profiles below threshold were also studied in [11]. These works motivate this letter.

The equations determining the spatial profile of a condensate are distinct for closed (conservative) and open (dissipative) systems. In a closed BEC, the Gross-Pitaevskii equation [29] (GPE), describes energy conserving phase evolution. In a purely dissipative system, the time dependent Ginzburg Landau equation [30] (GLE) describes irreversible relaxation. Combining these leads to the complex GPE or GLE [31], widely used for polariton condensates [32–34]. However, such equations can

only crudely model relaxation to a thermal state. Extensions have been developed [35, 36] to address this for polaritons. In this letter we show that for weak coupling one can derive a tractable model combining spatial dynamics with energy relaxation. This model describes how the spatial profile is determined by the competition between energy relaxation and loss, and can explain the recent experiments [27, 28].

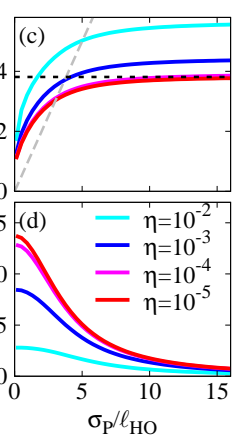
The photon BEC system consists of dye molecules (modeled as two-level systems) coupled to photon modes in an optical cavity. To incorporate inhomogeneous pumping we must consider the overlap  $\psi_m(\mathbf{r}_i)$  between the transverse mode function of photon mode  $m$  and a molecule at  $\mathbf{r}_i$ . Curvature of the cavity mirrors leads to an in-plane harmonic trap, so that  $\psi_m(\mathbf{r})$  are Gauss-Hermite functions in two dimensions and the corresponding frequencies are harmonically spaced,  $\omega_m = \omega_c + (m_x + m_y)\epsilon$ , where  $m$  combines both  $m_x$  and  $m_y$  indices. The “cavity cutoff”  $\omega_c$  is set by the cavity length. We write the master equation describing the system as two terms,  $\partial_t \hat{\rho} = \mathcal{M}_0[\hat{\rho}] + \mathcal{M}_{\text{int}}[\hat{\rho}]$ . The bare part is:

$$\mathcal{M}_0[\hat{\rho}] = -i \sum_m [\omega_m \hat{a}_m^\dagger \hat{a}_m, \hat{\rho}] + \sum_m \frac{\kappa}{2} \mathcal{L}[\hat{a}_m] + \sum_i \frac{\Gamma_\uparrow(\mathbf{r}_i)}{2} \mathcal{L}[\hat{\sigma}_i^+] + \sum_i \frac{\Gamma_\downarrow}{2} \mathcal{L}[\hat{\sigma}_i^-], \quad (1)$$

where  $\mathcal{L}[\hat{X}] = 2\hat{X}^\dagger \hat{\rho} \hat{X} - [\hat{X}^\dagger \hat{X}, \hat{\rho}]_+$ . The operator  $\hat{a}_m^\dagger$  creates a photon in mode  $m$ , and we assume all modes have decay rate  $\kappa$ . The electronic state of molecule  $i$  is represented by Pauli matrices  $\hat{\sigma}_i^{x,y,z}$ . In addition to coupling to the cavity (see below), each molecule has a pumping rate  $\Gamma_\uparrow(\mathbf{r}_i)$ , and a non-cavity decay rate  $\Gamma_\downarrow$  incorporating fluorescence into all modes other than the confined cavity modes. Other than the inhomogeneous pump,  $\mathcal{M}_0[\hat{\rho}]$  matches Refs. [16, 23]. The term  $\mathcal{M}_{\text{int}}[\hat{\rho}]$  can be treated at various levels of approximation. The most complete form is:

$$\mathcal{M}_{\text{int}}^{\text{full}}[\hat{\rho}] = \sum_{m,m',i} \psi_m^*(\mathbf{r}_i) \psi_{m'}(\mathbf{r}_i) \{ K(\delta_{m'}) [\hat{a}_{m'} \hat{\sigma}_i^+ \hat{\rho}, \hat{a}_m^\dagger \hat{\sigma}_i^-] + K(-\delta_{m'}) [\hat{a}_m^\dagger \hat{\sigma}_i^- \hat{\rho}, \hat{a}_{m'} \hat{\sigma}_i^+] \} + \text{H.c.} \quad (2)$$

The complex function  $K(\pm \delta_m)$ , discussed below, encodes



the molecular absorption (emission) rate vs. the detuning  $\delta_m = \omega_m - \omega_{ZPL}$  between mode  $m$  and the molecular “Zero Phonon Line” (see dashed line in Fig. 1(a,b)).

Equation (2) includes coherence between photon modes, but neglects coherence between molecules. This is because dye and solvent molecules collide frequently causing rapid dephasing. Inter-mode coherence is crucial to understand the dynamics, as studied experimentally in Ref. [28]. However, including inter-mode coherence is numerically expensive, and is only necessary when significant coherence exists. For the first part of this paper we consider instead a “diagonal approximation”,  $\mathcal{M}_{\text{int}}[\hat{\rho}] = \mathcal{M}_{\text{int}}^{\text{diag}}[\hat{\rho}] \equiv \frac{1}{2} \sum_{m,i} |\psi_m(\mathbf{r}_i)|^2 (\Gamma(\delta_m) \mathcal{L}[\hat{a}_m \hat{\sigma}_i^+] + \Gamma(-\delta_m) \mathcal{L}[\hat{a}_m^\dagger \hat{\sigma}_i^-]) - i[H_\Lambda, \hat{\rho}]$ , where  $\Gamma(\pm\delta) \equiv 2\Re[K(\pm\delta)]$  are the absorption(emission) rates, and  $H_\Lambda$  is a Lamb shift from the imaginary part of  $K(\pm\delta)$ .

For simple molecules,  $K(\delta)$  can be calculated explicitly [23]. Alternatively, one may use experimentally measured spectra  $\Gamma(\delta)$ , and find  $K(\delta)$  by analytic continuation — causality requires that  $K(\delta)$  is analytic in the lower half plane. As noted previously [10, 11, 16], thermalization of photons requires that  $\Gamma(\delta)$  obeys the Kennard-Stepanov (KS) relation [37–39],  $\Gamma(\delta) = \Gamma(-\delta)e^{\beta\delta}$ . We therefore use a function  $\Gamma(\delta)$ , shown in Fig. 1, that fits the experimental spectra, while satisfying the KS relation. This determines  $\Gamma(\delta)$  up to a prefactor. We denote  $\Gamma_{\text{max}} = \max[\Gamma(\delta)]$ , and discuss below how to estimate  $\Gamma_{\text{max}}$  from experimental results.

Typical experimental observables are the photon spectrum, and the density profile  $I(\mathbf{r})$  which is our focus in this letter. To derive  $I(\mathbf{r})$  starting from the master equation, we write equations of motion for the (Hermitian) photon correlation matrix  $[\mathbf{n}]_{m,m'} = \langle \hat{a}_m^\dagger \hat{a}_{m'} \rangle$ , and the coarse-grained excitation density,  $f(\mathbf{r}) = \sum_i \delta(\mathbf{r} - \mathbf{r}_i) \langle \hat{\sigma}_i^+ \hat{\sigma}_i^- \rangle$ . The photon density is then given by  $I(\mathbf{r}) = \sum_{m,m'} \psi_m^*(\mathbf{r}) \psi_{m'}(\mathbf{r}) [\mathbf{n}]_{m,m'}$ . Within the semiclassical approximation [23]  $[\mathbf{n}]_{m,m'}$  and  $f(\mathbf{r})$  obey a closed set of equations. In this diagonal approximation the correlation matrix takes the form  $[\mathbf{n}]_{m,m'} = n_m \delta_{m,m'}$  and:

$$\partial_t n_m = \rho_0 \Gamma(-\delta_m) f_m (n_m + 1) - [\kappa + \rho_0 \Gamma(\delta_m) (1 - f_m)] n_m, \quad (3)$$

$$\partial_t f(\mathbf{r}) = -\Gamma_{\downarrow}^{\text{tot}}(n_m, \mathbf{r}) f(\mathbf{r}) + \Gamma_{\downarrow}^{\text{tot}}(n_m, \mathbf{r}) (1 - f(\mathbf{r})), \quad (4)$$

where  $f_m = \int d^d \mathbf{r} f(\mathbf{r}) |\psi_m(\mathbf{r})|^2$  defines the gain for mode  $m$ , and  $\rho_0$  is the molecular density. The “total” molecular excitation and decay rates, including the  $\mathbf{r}$  dependent emission into cavity modes, are:

$$\Gamma_{\downarrow}^{\text{tot}}(n_m, \mathbf{r}) = \Gamma_{\downarrow} + \sum_m |\psi_m(\mathbf{r})|^2 \Gamma(-\delta_m) (n_m + 1), \quad (5)$$

$$\Gamma_{\uparrow}^{\text{tot}}(n_m, \mathbf{r}) = \Gamma_{\uparrow}(\mathbf{r}) + \sum_m |\psi_m(\mathbf{r})|^2 \Gamma(\delta_m) n_m. \quad (6)$$

In the following we explore the consequences of a finite size Gaussian pump spot,  $\Gamma_{\uparrow}(\mathbf{r}) = \Gamma_{\uparrow}^{\text{int}} \exp[-(\mathbf{r} -$

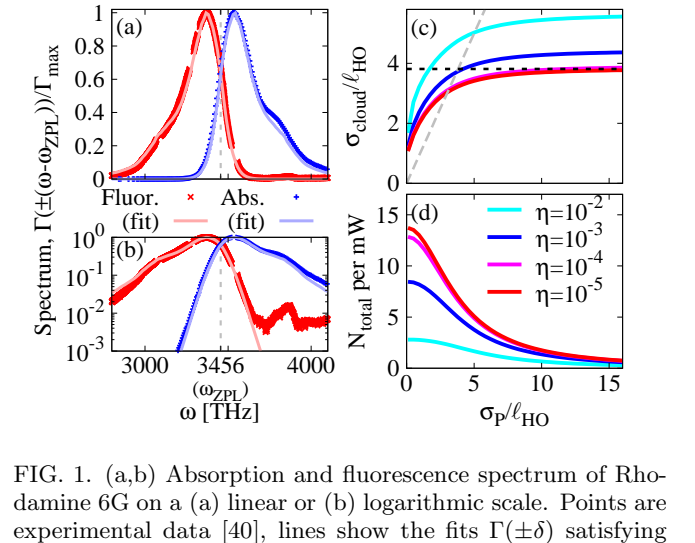


FIG. 1. (a,b) Absorption and fluorescence spectrum of Rhodamine 6G on a (a) linear or (b) logarithmic scale. Points are experimental data [40], lines show the fits  $\Gamma(\pm\delta)$  satisfying  $\Gamma(\delta) = \Gamma(-\delta)e^{\beta\delta}$  at room temperature. Here and throughout, we plot angular frequency,  $\omega = 2\pi f$ . (c) Photon cloud size and (d) photon number (per unit power) vs pump-spot size, for various  $\eta \equiv \kappa/\rho_0 \Gamma_{\text{max}}$ . Panels (c,d) for  $d = 2$ , far below threshold using Eq. (7) with  $\omega_c = 3200\text{THz}$ . Dashed lines in (c) show thermal size  $\sigma_T$  (see text) and pump size  $\sigma_P$ .

$\mathbf{r}_P]^2 / 2\sigma_P^2) / (2\pi\sigma_P^2)^{d/2}$ , where  $\Gamma_{\uparrow}^{\text{int}}$  is the integrated intensity,  $\sigma_P$  the spot size,  $\mathbf{r}_P$  the offset, and  $d$  the dimension. Note that  $\Gamma_{\uparrow}^{\text{int}}$  has units of  $[T]^{-1}[L]^d$ . Similarly, since  $\Gamma(\pm\delta)$  are multiplied by  $\rho_0$  or  $|\psi_m(\mathbf{r})|^2$ , this means  $\Gamma_{\text{max}}$  also has units  $[T]^{-1}[L]^d$ . We measure all lengths (and densities) in units of the oscillator length  $\ell_{\text{HO}}$  of the harmonic trap potential. For comparison to Ref. [27], in the first part of this letter we set  $\mathbf{r}_P = 0$ .

Far below threshold, when  $\Gamma_{\uparrow}(\mathbf{r} = 0) \ll \Gamma_{\downarrow}$ , both  $n_m$  and  $f(\mathbf{r})$  are small, so the steady state of Eq. (3,4) is

$$f(\mathbf{r}) \simeq \frac{\Gamma_{\uparrow}(\mathbf{r})}{\Gamma_{\downarrow}^{\text{tot}}(n_m = 0, \mathbf{r})}, \quad n_m \simeq f_m \frac{\Gamma(-\delta_m)}{\Gamma(\delta_m) + \kappa/\rho_0}. \quad (7)$$

For relevant parameters (see below), the cavity mode contribution to  $\Gamma_{\downarrow}^{\text{tot}}(n_m = 0, \mathbf{r})$  is small, so  $f(\mathbf{r}) \simeq \Gamma_{\uparrow}(\mathbf{r})/\Gamma_{\downarrow}$ , and the overlaps  $f_m$  depend on the pump shape. In this limit the shape of  $I(\mathbf{r})$  depends on the shape of the pump, the normalized spectrum  $\Gamma(\pm\delta)/\Gamma_{\text{max}}$ , and  $\eta \equiv \kappa/\rho_0 \Gamma_{\text{max}}$ . If  $\eta \ll 1$  and the KS relation is obeyed then:  $n_m = f_m e^{-\beta\delta_m}$ . If one also has  $\sigma_P \gg \ell_{\text{HO}}$ , then  $f_m$  is independent of  $m$  and so there is a thermal photon distribution and  $I(\mathbf{r}) \propto \sum_m e^{-\beta\delta_m} |\psi_m(\mathbf{r})|^2 \propto \exp(-r^2/2\sigma_T^2)$  with  $\sigma_T = \ell_{\text{HO}} / \sqrt{2 \tanh(\beta\epsilon/2)}$ , which recovers the classical thermal cloud size if  $k_B T \gg \epsilon$ , see Fig. 1(c). Thermalization fails for small  $\sigma_P$  or large  $\eta$ . At small  $\sigma_P$  this failure is due to mode dependence of  $f_m$ : A small pump spot populates only the low order photon modes, leading to an unnaturally small (i.e. cold) photon cloud. Note that for this to occur, the presence of the non-cavity decay rate  $\Gamma_{\downarrow}$  is crucial. For large  $\eta$  thermalization fails because  $n_m \simeq f_m \Gamma(-\delta_m) / \kappa \rho_0$ , and no Boltzmann factor

arises. In Fig. 1(c) this gives a photon cloud which is larger than  $\sigma_T$ .

Figure 1(d) shows the total photon number (per incident power) vs pump spot size. For large spots, the number falls off as  $(\sigma_P)^{-d}$ . This is because for all modes  $m$  with extent much smaller than  $\sigma_P$ , one may approximate  $f_m \simeq \Gamma_{\uparrow}(\mathbf{r} = 0)/\Gamma_{\downarrow} = \Gamma_{\uparrow}^{\text{int}}/[\Gamma_{\downarrow}(\sqrt{2\pi}\sigma_P)^d]$ . In contrast, for small spots, the number saturates; here  $\sigma_P$  is much smaller than the extent of the relevant modes and so  $f_m \simeq |\psi_m(\mathbf{r} = 0)|^2\Gamma_{\uparrow}^{\text{int}}/\Gamma_{\downarrow}$ , independent of  $\sigma_P$ . In experiment [27], the total photon number initially increases with spot size, an effect not seen here.

The behavior in Fig. 1(c) for  $\eta \simeq 10^{-3}$  is very similar to the experimental results of Ref. [27]. Using other known parameters of this experiment,  $\rho_0 \simeq 10^8\ell_{\text{HO}}^{-2}$ , and  $\kappa = 500\text{MHz}$ , this gives  $\Gamma_{\text{max}} = 5\text{kHz}\ell_{\text{HO}}^2$ . Comparing the rate  $\Gamma(-\delta_m)|\psi_0(\mathbf{r} = 0)|^2 < \Gamma_{\text{max}}/(\sqrt{\pi}\ell_{\text{HO}}^2)$  to the observed background decay rate  $\Gamma_{\downarrow} \simeq 250\text{MHz}$ , this means stimulated emission into cavity modes is only dominant once  $n_m \gtrsim 10^4$ . We use these parameter values below unless otherwise stated.

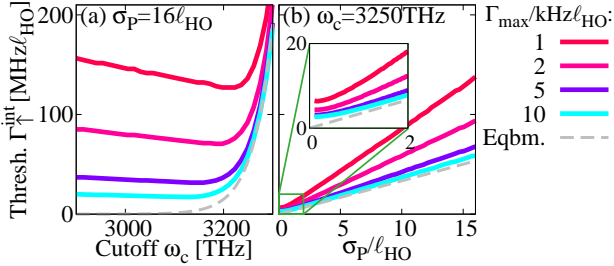


FIG. 2. Threshold (integrated) pump power, calculated in  $d = 1$  for various values of  $\Gamma_{\text{max}}$ . (a) vs cavity cutoff,  $\omega_c$ , (b) vs pump spot size. The dashed line shows the equilibrium result  $\Gamma_{\uparrow}(\mathbf{r} = 0) = \Gamma_{\downarrow}e^{\beta\delta_c}$ . At large spot sizes, the threshold power increases as  $(\sigma_P)^d$  and so is linear for this 1D simulation.

We next turn to the behavior at threshold [41], and explore how this depends on the pump size. Figure 2 shows the threshold value of  $\Gamma_{\uparrow}^{\text{int}}$  vs cavity cutoff,  $\omega_c$ , and vs pump spot size,  $\sigma_P$ . These calculations, solving Eq. (3–6) numerically, are computationally expensive in  $d = 2$  so we consider  $d = 1$  from hereon. In equilibrium the threshold condition is  $\Gamma_{\uparrow}(\mathbf{r} = 0) = \Gamma_{\downarrow}e^{\beta\delta_c}$ , where  $\delta_c = \omega_c - \omega_{ZPL}$  (see [16]). This condition has a simple meaning: it identifies when the effective chemical potential of the molecules,  $\mu_{\text{eff}}(\mathbf{r}) = k_B T \ln[\Gamma_{\uparrow}(\mathbf{r})/\Gamma_{\downarrow}]$  reaches the lowest photon mode [23]. This thermal prediction is shown as the dashed line in Fig. 2.

The actual threshold in Fig. 2(a) is however non-monotonic. At large  $\omega_c$  the system is thermal, and so threshold increases exponentially with  $\omega_c$ . At small  $\omega_c$  the absorption and emission rates are too small to compete with cavity loss, and so the threshold pump increases. Such non-monotonic dependence has been seen experimentally [27]. The minimum of threshold becomes

more pronounced as one increases the cavity loss rate  $\kappa$  or decreases the peak emission rate  $\Gamma_{\text{max}}$ . In Fig. 2(b), we see  $\Gamma_{\uparrow}^{\text{int}} \propto (\sigma_P)^d$  at threshold, except for small spot sizes where it saturates. This dependence on spot size occurs because threshold is reached first at the trap center, where  $\mu_{\text{eff}}(\mathbf{r})$  is greatest. As such, it is the peak pump power  $\propto \Gamma_{\text{max}}^{\text{int}}\sigma_P^{-d}$  that enters the threshold condition.

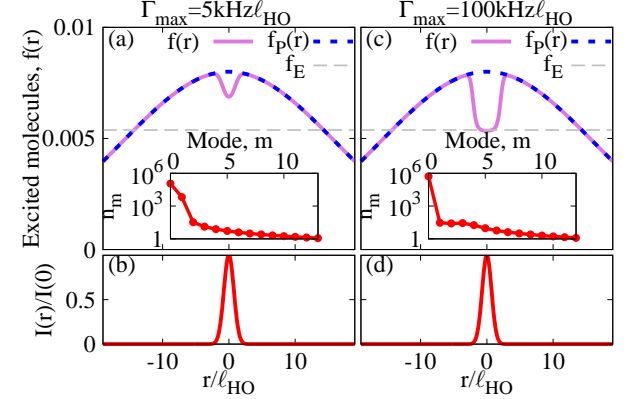


FIG. 3. Clamping of the gain profile for sufficiently large  $\Gamma_{\text{max}}$  (in  $d = 1$ ). Panels (a,b) show  $\Gamma_{\text{max}} = 5\text{kHz}\ell_{\text{HO}}$ , panels (c,d)  $\Gamma_{\text{max}} = 100\text{kHz}\ell_{\text{HO}}$ . Top panels show the gain profile  $f(\mathbf{r})$  (solid), the value set by the pump,  $f_P(\mathbf{r}) = \Gamma_{\uparrow}(\mathbf{r})/(\Gamma_{\downarrow} + \Gamma_{\uparrow}(\mathbf{r}))$  (short dashed), and the clamped value  $f_E = [e^{-\beta\delta_c} + 1]^{-1}$  for the cavity cutoff  $\omega_c = 3200\text{THz}$ . Bottom panels show the (normalized) photon density. Insets show the mode populations  $n_m$ , demonstrating multimode condensation.

Once threshold is reached, in equilibrium, the chemical potential locks at  $\mu_{\text{eff}} = \delta_c$ . This means that the “gain profile”  $f(\mathbf{r})$ , i.e. the fraction of excited molecules, must saturate,  $f(\mathbf{r}) \leq f_E = [e^{-\beta\delta_c} + 1]^{-1}$ . Thus, for a photon BEC, the laser concept of gain clamping and the thermal concept of chemical potential locking are the same. This also implies  $f(\mathbf{r})$  should become uniform at threshold, and we next turn to explore if and how this occurs. Figure 3 shows  $f(\mathbf{r})$  slightly above threshold for two values of  $\Gamma_{\text{max}}$ . At  $\Gamma_{\text{max}} = 100\text{kHz}\ell_{\text{HO}}$ , clamping is seen near the trap center, but for  $\Gamma_{\text{max}} = 5\text{kHz}\ell_{\text{HO}}$  it is absent. The dependence on  $\Gamma_{\text{max}}$  follows from the steady state result,  $f(\mathbf{r}) = [\Gamma_{\downarrow}^{\text{tot}}(\mathbf{r})/\Gamma_{\uparrow}^{\text{tot}}(\mathbf{r}) + 1]^{-1}$  and the form of  $\Gamma_{\uparrow,\downarrow}^{\text{tot}}(\mathbf{r})$  in Eq. (5,6). If  $n_m$  is a Bose-Einstein distribution with chemical potential  $\mu$  and  $\Gamma(\delta)$  obeys the KS relation then  $\Gamma(-\delta_m)(n_m + 1) = \Gamma(\delta_m)n_m e^{-\beta\mu}$ . This means that if  $\sum_m |\psi_m(\mathbf{r})|^2 \Gamma(-\delta_m)(n_m + 1) \gg \Gamma_{\downarrow}$  and  $\sum_m |\psi_m(\mathbf{r})|^2 \Gamma(\delta_m)n_m \gg \Gamma_{\uparrow}(\mathbf{r})$  then one has an uniform gain profile  $f(\mathbf{r}) = f_E$ . We thus see that gain clamping requires large  $\Gamma(\pm\delta)$ . Moreover, since the condensed mode(s) are concentrated at the trap center, gain clamping is spatially restricted, as seen in Fig. 3(c). In the terminology of lasers, this is spatial hole burning [42].

As the gain clamping is imperfect, other modes may reach threshold leading to multimode condensation. In Fig. 3 the inset shows the mode populations  $n_m$ , demon-

strating that several modes are macroscopically occupied. For values of  $\Gamma_{\max}$  larger than those shown, multimode condensation is suppressed. Both the inhomogeneous  $f(\mathbf{r})$  and multimode condensation are signatures of imperfect thermal equilibrium. An interesting question for future work is how such hole burning might be used to engineer the photon condensate profile.

So far, we have focused on steady states. Schmitt *et al.* [28] studied the dynamics after an off-center pump pulse and observed oscillations of the photon condensate. To describe oscillations requires that we reintroduce inter-mode coherences, allowing beating between modes. We therefore time-evolve the full photon correlation matrix  $[\mathbf{n}]_{m,m'}$  using  $\mathcal{M}_{\text{int}}[\hat{\rho}] = \mathcal{M}_{\text{int}}^{\text{full}}[\hat{\rho}]$ . Including inter-mode coherences, the semiclassical equations take a compact form if we define the matrices  $[\mathbf{K}_{\pm}]_{m,m'} \equiv \delta_{m,m'} K(\pm \delta_m)$ , the mode function matrix  $[\Psi(\mathbf{r})]_{m,m'} \equiv \psi_m(\mathbf{r})\psi_{m'}(\mathbf{r})$ , the overlap matrix  $\mathbf{f} \equiv \int d^d\mathbf{r} f(\mathbf{r})\Psi(\mathbf{r})$  and  $[\mathbf{h}]_{m,m'} \equiv \delta_{m,m'}(i\omega_m - \kappa)$ . We thus find the matrix equation:

$$\partial_t \mathbf{n} = \left( \mathbf{h} + \mathbf{f}[\mathbf{K}_- + \mathbf{K}_+^\dagger] - \mathbf{K}_+^\dagger \right) \mathbf{n} + \mathbf{f}\mathbf{K}_- + \text{H.c.} \quad (8)$$

The gain profile  $f(\mathbf{r})$  still obeys Eq. (4), but now the total rates are given by  $\Gamma_{\uparrow}^{\text{tot}}(\mathbf{r}) = \Gamma_{\uparrow}(\mathbf{r}) + 2\Re(\text{Tr}[\Psi(\mathbf{r})\mathbf{n}\mathbf{K}_+])$  and  $\Gamma_{\downarrow}^{\text{tot}}(\mathbf{r}) = \Gamma_{\downarrow} + 2\Re(\text{Tr}[\Psi(\mathbf{r})\mathbf{K}_-(\mathbf{n} + \mathbf{1})])$ .

By including inter-mode coherences, our equations no longer make the “secular approximation”, which discards those bath-induced terms which are time dependent in the interaction picture. In our model the secular approximation is identical to the diagonal approximation. The secular approximation is often introduced as a necessary condition for having a completely positive master equation [43]. However several recent papers suggest the secular approximation can lead to incorrect predictions [44–46]. The current model falls into this class: the *experimentally observed* oscillations of the photon density can only occur if the molecular emission produces inter-mode coherence — an incoherent state would show no beating. Beyond the secular approximation, there may be instabilities, particularly at large  $\Gamma_{\max}$ . However, for large  $\Gamma_{\max}$  the Markov approximation fails [46]. For the parameters we consider, our equations are stable.

Figure 4 shows the dynamics following a short, high intensity, off-center pump pulse. The behavior differs according to the cavity cutoff  $\omega_c$  as seen experimentally [28]. Oscillations occur initially in both cases, but at late times, they are replaced by a nearly thermal condensate if  $\omega_c$  is large enough. Note that, as seen in experiment, the switch to the thermal condensate does not occur through a continuous damping of the amplitude of the oscillations. Because our simulations also determine the gain profile  $f(\mathbf{r})$ , one may see that thermalization occurs when re-absorption of photons leads to a flat gain profile  $f(\mathbf{r}) \simeq f_E$  in the center of the trap. For smaller  $\omega_c$ , reabsorption is too weak to produce this effect.

In conclusion, we have presented a theoretical model

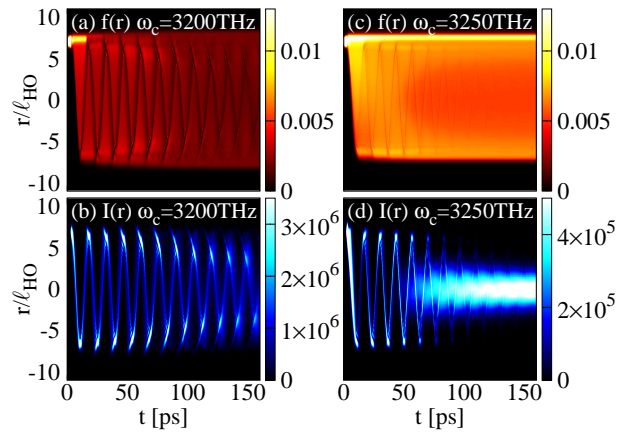


FIG. 4. Oscillations following an off-center pump pulse (in  $d = 1$ ). Panels (a,b) are for  $\omega_c = 3200\text{THz}$ , where thermalization is not sufficient to suppress the oscillations. Panels (c,d) are for  $\omega_c = 3250\text{THz}$ , showing thermalization at late times. Panels (a,c) show  $f(\mathbf{r})$ , and (b,d) show  $I(\mathbf{r})$ . The pump pulse is a Gaussian at  $r_P = 7\ell_{\text{HO}}$ , with width  $\sigma_P = 0.3\ell_{\text{HO}}$ , duration duration 5ps and intensity  $\Gamma_{\uparrow}^{\text{int}} = 24\text{GHz}\ell_{\text{HO}}$ . Other parameters;  $\kappa = 100\text{MHz}$ ,  $\Gamma_{\downarrow} = 250\text{MHz}$ ,  $\Gamma_{\max} = 3\text{MHz}\ell_{\text{HO}}$ , mode spacing  $\epsilon = 0.4\text{THz}$ . These last two parameters are enhanced compared to experiments to reduce simulation time.

capable of describing the spatial dynamics, relaxation, and thermalization of an inhomogeneously pumped photon condensate. Using this, we have reproduced recent experimental results studying the effects of small pump spots. Even without photon loss, thermalization can be inhibited by small spot size. Our model gives direct access to the gain profile  $f(\mathbf{r})$ , which is hard to access experimentally. By doing so, we see the observed behavior is related to gain clamping and spatial hole burning. Such phenomena have recently prompted significant interest in other contexts, e.g. for random lasers [47, 48], where the role of mode competition and the statistics of multimode lasing have been studied. Mode competition is the basis of transverse pattern formation in nonlinear optics [3, 49], and is a prime example of pattern formation out of equilibrium [50]. The results presented in this paper provide the foundation to study these effects in the photon condensate.

We are very happy to acknowledge stimulating discussions with R. A. Nyman, J. Klärs, M. Weitz and V. Oganesyan. We also wish to thank R. Nyman for providing the measured absorption and luminescence data shown in Fig. 1. The authors acknowledge financial support from EPSRC program “TOPNES” (EP/I031014/1) and EPSRC (EP/G004714/2). JK acknowledges support from the Leverhulme Trust (IAF-2014-025). PGK acknowledges support from EPSRC (EP/M010910/1).

---

[1] R. Graham and H. Haken, *Z. Phys.* **237**, 31 (1970).

[2] H. Haken, *Rev. Mod. Phys.* **47**, 67 (1975).

[3] K. Staliunas and V. J. Sanchez-Morcillo, *Transverse Patterns in Nonlinear Optical Resonators* (Springer-Verlag, Berlin, 2003).

[4] J. Kasprzak, M. Richard, S. Kundermann, A. Baas, P. Jeambrun, J. M. J. Keeling, F. M. Marchetti, M. H. Szymaska, R. André, J. L. Staehli, V. Savona, P. B. Littlewood, B. Deveaud, and L. S. Dang, *Nature* **443**, 409 (2006).

[5] R. Balili, V. Hartwell, D. Snoke, L. Pfeiffer, and K. West, *Science* **316**, 1007 (2007).

[6] I. Carusotto and C. Ciuti, *Rev. Mod. Phys.* **85**, 299 (2013).

[7] P. C. Hohenberg and B. I. Halperin, *Rev. Mod. Phys.* **49**, 435 (1977).

[8] L. M. Sieberer, S. D. Huber, E. Altman, and S. Diehl, *Phys. Rev. Lett.* **110**, 195301 (2013).

[9] E. Altman, L. M. Sieberer, L. Chen, S. Diehl, and J. Toner, *Phys. Rev. X* **5**, 011017 (2015).

[10] J. Klaers, J. Schmitt, F. Vewinger, and M. Weitz, *Nature* **468**, 545 (2010).

[11] J. Klaers, F. Vewinger, and M. Weitz, *Nat. Phys.* **6**, 512 (2010).

[12] F. P. Schäfer, ed., *Dye Lasers*, 3rd ed. (Springer-Verlag, 1990).

[13] J. Klaers, J. Schmitt, T. Damm, F. Vewinger, and M. Weitz, *Phys. Rev. Lett.* **108**, 160403 (2012).

[14] D. N. Sob'yanin, *Phys. Rev. E* **85**, 061120 (2012).

[15] D. W. Snoke and S. M. Girvin, *J. Low Temp. Phys.* **171**, 1 (2013).

[16] P. Kirton and J. Keeling, *Phys. Rev. Lett.* **111**, 100404 (2013).

[17] A. Kruchkov, *Phys. Rev. A* **89**, 033862 (2014).

[18] E. C. I. van der Wurff, A.-W. de Leeuw, R. A. Duine, and H. T. C. Stoof, *Phys. Rev. Lett.* **113**, 135301 (2014).

[19] A.-W. de Leeuw, H. T. C. Stoof, and R. A. Duine, *Phys. Rev. A* **89**, 053627 (2014).

[20] A. Chiocchetta and I. Carusotto, *Phys. Rev. A* **90**, 023633 (2014).

[21] R. A. Nyman and M. H. Szymaska, *Phys. Rev. A* **89**, 033844 (2014).

[22] E. Sela, A. Rosch, and V. Fleurov, *Phys. Rev. A* **89**, 043844 (2014).

[23] P. Kirton and J. Keeling, *Phys. Rev. A* **91**, 033826 (2015).

[24] A. W. de Leeuw, E. C. I. van der Wurff, R. A. Duine, and H. T. C. Stoof, *Phys. Rev. A* **90**, 043627 (2015).

[25] A. Chiocchetta, A. Gambassi, and I. Carusotto, (2015), arXiv:1503.02816.

[26] J. Schmitt, T. Damm, D. Dung, F. Vewinger, J. Klaers, and M. Weitz, *Phys. Rev. Lett.* **112**, 030401 (2014).

[27] J. Marelic and R. A. Nyman, *Phys. Rev. A* **91**, 033813 (2015).

[28] J. Schmitt, T. Damm, D. Dung, F. Vewinger, J. Klaers, and M. Weitz, (2014), arXiv:1410.5713.

[29] L. P. Pitaevskii and S. Stringari, *Bose-Einstein Condensation* (Clarendon Press, Oxford, 2003).

[30] V. L. Ginzburg and L. D. Landau, *Zh. Eksp. Teor. Fiz.* **20**, 1064 (1950).

[31] I. Aranson and L. Kramer, *Rev. Mod. Phys.* **74**, 99 (2002).

[32] M. Wouters and I. Carusotto, *Phys. Rev. Lett.* **99**, 140402 (2007).

[33] J. Keeling and N. G. Berloff, *Phys. Rev. Lett.* **100**, 250401 (2008).

[34] M. Wouters, I. Carusotto, and C. Ciuti, *Phys. Rev. B* **77**, 115340 (2008).

[35] M. Wouters, T. C. H. Liew, and V. Savona, *Phys. Rev. B* **82**, 245315 (2010).

[36] M. Wouters, *New J. Phys.* **14**, 075020 (2012).

[37] E. H. Kennard, *Phys. Rev.* **11**, 29 (1918).

[38] E. H. Kennard, *Phys. Rev.* **28**, 672 (1926).

[39] B. I. Stepanov, *Dokl. Akad. Nauk SSSR* **112**, 839 (1957).

[40] R. A. Nyman and J. Marelic, Private Communication. The absorption spectrum is a composite at several concentrations, to improve the accuracy around 3200 THz.

[41] As with any finite size system, the threshold is not perfectly sharp; for definiteness we use the same threshold condition defined in Refs. [16, 23].

[42] A. E. Siegman, *Lasers* (University Science Books, Sausalito, 1986).

[43] R. Dümcke and H. Spohn, *Zeitschrift für Phys. B* **34**, 419 (1979).

[44] J. Jeske, D. Ing, M. B. Plenio, S. F. Huelga, and J. H. Cole, *J. Chem. Phys.* **142**, 064104 (2015).

[45] C. Joshi, P. Ohberg, J. D. Cresser, and E. Andersson, *Phys. Rev. A* **90**, 063815 (2015).

[46] P. Eastham, P. Kirton, H. Cammack, B. W. Lovett, and J. Keeling, “Bath induced coherence and the secular approximation,” In preparation.

[47] H. E. Türeci, A. D. Stone, L. Ge, S. Rotter, and R. J. Tandy, *Nonlinearity* **22**, C1 (2008).

[48] L. Ge, Y. D. Chong, and A. D. Stone, *Phys. Rev. A* **82**, 063824 (2010).

[49] C. Denz, M. Schwab, and C. Weilnau, *Transverse-Pattern Formation in Photorefractive Optics*, Springer Tracts in Modern Physics, Vol. 188 (Springer-Verlag, Berlin, 2003).

[50] M. C. Cross and P. C. Hohenberg, *Rev. Mod. Phys.* **65**, 851 (1993).